Advancing Inkjet-Printed Electroluminescent Quantum-Dot Displays Toward Commercialization: Improving Blue EL-QD Lifetime

*Sehun Kim†, Changyeol Han†, Heunggyu Kim†, Jungho Jo†, Sooho Lee†, Jonghoon Kim†, Myoungjin Park†, Sanghee Yu†, Gyubong Kim†, Hoilim Kim†, Arong Lee†, Kyeongseo Min†, Giho Kang†, Jee Hoon Park†, Jaekwon Hwang†, Ji Hyun Min‡, Hyun Dong Ha‡, Yongseok Han‡, Da-Eun Yoon‡, Hogeun Chang‡, Kwang-Hee Kim‡, Sungwoo Kim‡, Jaehyun Park†, Seunguk Noh†, Donghoon Kwak†, Youngmo Koo†, Jaekook Ha†, Yeo-geon Yoon† and Changhee Lee†,**

† Display Research Center, Samsung Display Co., Ltd., Giheung-gu, Yongin-City, Gyeonggi-Do, Korea
‡ Samsung Advanced Institute of Technology, Samsung Electronics, Suwon, South Korea

Abstract

One of the primary challenges in commercializing electroluminescent quantum dot (EL-QD) displays is the limited operational lifetime of blue-emitting devices. To address this, we explored various strategies focusing on optimization of both materials and inkjet printing processes. The efficiency and lifetime of blue EL-QD devices are significantly improved through ligand engineering of ZnSeTe QDs and defect control in ZnMgO nanoparticles. We successfully demonstrate an all-inkjet-printed 18.2-inch full-color EL-QD display with a resolution of 202 ppi.

Author Keywords

Cd-free quantum dots (QDs), Electroluminescent quantum dot (EL-QD) devices, Quantum dot light-emitting diode displays (QD-LEDs), Ligand engineering, Inkjet printing process.

1. Introduction

Colloidal quantum dots (QDs) are nanometer-sized semiconductor crystals that operate within the quantum confinement regime. Due to their size- and composition-dependent bandgap tunability, narrow emission bandwidth, and near-unity photoluminescence quantum yields (PLQY), QDs have been extensively studied over the past few decades [1-6]. Notably, the solution processability of QDs, combined with their high dispersion stability, enables cost-effective manufacturing based on inkjet printing technology, positioning QD-based displays as next-generation high-performance displays.

The performance of QD-based displays has seen significant improvements, driven by advances in QD synthesis methods and device engineering. For example, in red and green InP QD-based light-emitting diodes (QD-LEDs), key strategies include achieving regular morphologies and optimizing charge balance by forming thin ZnS shells. Won *et al*. demonstrated a red-emitting QD-LED with an external quantum efficiency (EQE) of 21.4% and a T_{50} lifetime of 1,000,000 hours at 100 nits by precisely controlling the random facets of QDs and applying a 0.3 monolayer (ML) thin ZnS layer [7]. Similarly, Yu *et al*. achieved a green-emitting QD-LED with an EQE of 15.2% by optimizing the Se-to-S ratio in ZnSeS alloy shells [8]. Increased Se content raised the valence band maximum, facilitating hole injection in the devices. While these advancements have resulted in highly efficient red and green InP QD-LEDs, research on ZnSeTe-based QD-LEDs, which are promising eco-friendly candidates for blue emission, remains limited.

The intrinsic properties of ZnSeTe QDs, particularly the high degree of electron delocalization across their volume, present challenges for blue-emitting QD-LED development. Unlike InP QDs, the significant electron delocalization in ZnSeTe necessitates thicker ZnS shells to achieve electron confinement. However, this increased thickness often leads to charge accumulation at the interface between QDs and electron transport layer (ETL), negatively impacting the device lifetime. Overcoming these intrinsic properties requires alternative strategies beyond those used for InP QDs to achieve highly stable and efficient blue ZnSeTe-based QD-LEDs [6, 9].

ZnMgO nanocrystals (NCs) are commonly used as an ETL for QD-LEDs. Intrinsic defects in ZnMgO can enhance charge transfer at heterointerfaces by providing favorable energy states for charges, but they facilitate chemical interactions. Employing electrochemically stable ligands for ZnMgO surface functionalization has been shown to improve the device performance by suppressing interfacial charge transfer between QDs and ETLs [10]. Ghorbani et al. reported that the primary cause of electroluminescence (EL) loss in blue QDs is not PLQY degradation but rather changes in charge injection dynamics [11]. Electrical analysis of electron-only devices (EODs) and hole-only devices (HODs) revealed that hole injection into blue QDs increases over time, while electron injection decreases, leading to charge imbalance and performance deterioration.

In this study, we present highly efficient and stable blue EL-QDs achieved through ligand engineering and surface defect control. By optimizing the ratio of long- and short-chain ligands, we mitigate charge accumulation at the QD/ETL interface, even in the presence of energy barriers introduced by thick ZnS shells. Furthermore, the incorporation of metal halides was found to suppress positive charge accumulation and reduce defect formation (e.g., oxygen vacancies) in ZnMgO, significantly enhancing QD-LED lifetime. These findings underscore the critical role of ligand engineering in advancing the performance and stability of blue EL-QD devices, paving the way for their commercialization in next-generation displays.

2. Results and Discussion

To enhance the performance of blue QD- LEDs, we explored various strategies involving both material and device architecture. Blue-emitting ZnSeTe QDs (BQDs) were synthesized by tuning the Te/Se ratio and controlling the shell thickness. Transmission electron microscopy (TEM) images reveal that the QDs exhibit cubic or tetrahedral morphologies with well-developed (100) or (111) facets and an average size of 9.5 nm, as shown in Figure 1(a). The as-synthesized QDs (QD-A) demonstrated excellent dispersibility in the ink system,

ISSN 0097-996X/25/5601-0227-$1.00 © 2025

attributed to the presence of oleic acid (OA) ligands on their surface. While OA's long carbon chain enhances dispersibility, it impedes charge injection in electroluminescent devices. To overcome this limitation, we introduced a shorter-chain ligand (Ligand-A) to facilitate charge injection. However, replacing all OA with Ligand-A led to insufficient steric hindrance, making it challenging to maintain dispersibility in the ink solvent. Therefore, we synthesized QD-B by partially replacing OA with Ligand-A, achieving balance that preserved dispersibility and improved charge injection. To confirm the ligand composition on the QD surface, gas chromatography/mass spectrometry (GC/MS) analysis was conducted, and the relative proportions of each ligand were determined by comparing signal areas, as presented in Table 1. The analysis result confirmed the final ligand composition on QD-B's surface closely matched the intended feeding ratio of 85:15 (OA:Ligand-A), with an actual ratio of 88:12 (Table 1). The TEM image of QD-B (Figure 1(b)) showed negligible changes compared to QD-A, indicating structural consistency.

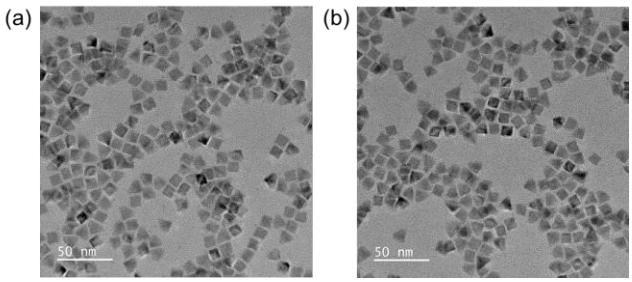

Figure 1. TEM images of (a) as-synthesized QDs (QD-A) and (b) QD-B synthesized by partially replacing OA with Ligand-A.

Table 1. Ratio of the ligands on QDs analyzed by gas chromatography/mass spectrometry (GC/MS)

QD	Ligand	Feeding ratio	Relative ratio on QD surface
QD-A	OA	100%	100%
	Ligand-A	-	-
QD-B	OA	85%	88%
	Ligand-A	15%	12%

To evaluate the influence of ligand modification on charge transport, electron-only devices (EODs) and hole-only devices (HODs) were fabricated. The device architectures for EODs and HODs were ZnMgO / BQD / ZnMgO / AgMg and HIL / HTL / BQD / HAT-CN / Ag, respectively, where HAT-CN is 1,4,5,8,9, 1 1-hexaazatriphenylene hexacarbonitrile. At a current density of 5 mA/cm^2, EODs incorporating QD-A exhibited a voltage of 2.2 V, while HODs required 7.4 V, indicating more efficient electron injection compared to hole injection. For QD-B, the EOD voltage increased to 9.3 V, whereas the HOD voltage decreased to 4.8 V, demonstrating improved hole transport (Figure 2). These results underscore the effectiveness of ligand engineering in modulating charge transport properties.

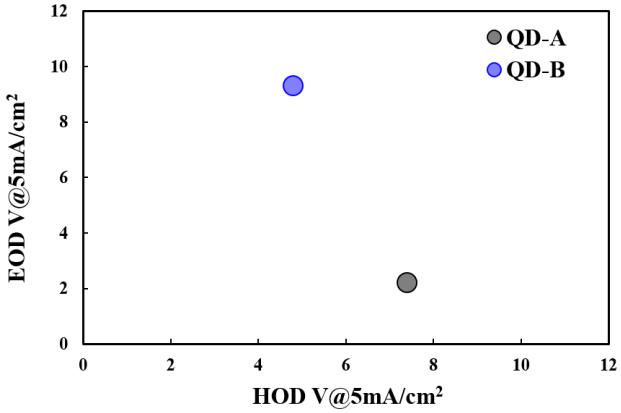

Figure 2. Voltages at a current density of 5mA/cm^2 of electron-only-devices (EODs) and hole-only-devices (HODs) employing QD-A or QD-B in the EML, respectively.

The blue EL-QD devices were constructed through spin-coating process using ink-jet printable inks (HIL, ZnMgO, ETL). The device structure was optimized to the top-emission architecture of ITO (substrate) / HIL / HTL / BQD / ZnMgO ETL / cathode (AgMg) / CPL (Capping layer) (Figure 3). Devices A and B were fabricated with QD-A and QD-B, respectively. The current density-voltage (J-V) curve for Device B shifted toward higher voltages (Figure 4(a)), but it achieved enhanced operational lifetime despite lower efficiency compared to Device A (Figures 4(b) and 4(c)). Further optimization was conducted by varying the emissive layer (EML) thickness in Device B to create variants: Device C (intermediate thickness) and Device D (thicker EML). As the EML thickness increases, the J-V curve shifted toward higher voltages. While Device D' s excessive thickness hindered charge injection and reduced efficiency, Device C achieved a balance, maintaining consistent efficiency across luminance levels and significantly extending operational lifetime. These improvements were attributed to enhanced charge balance at optimal EML thickness.

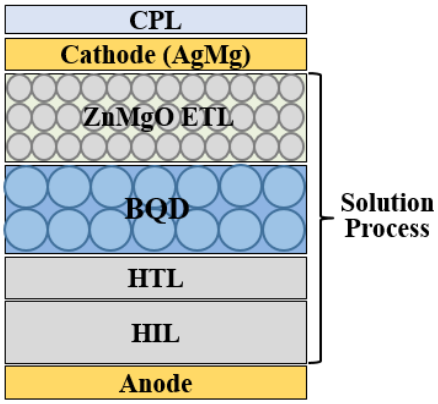

Figure 3. A schematic diagram of the architecture of blue EL-QD devices.

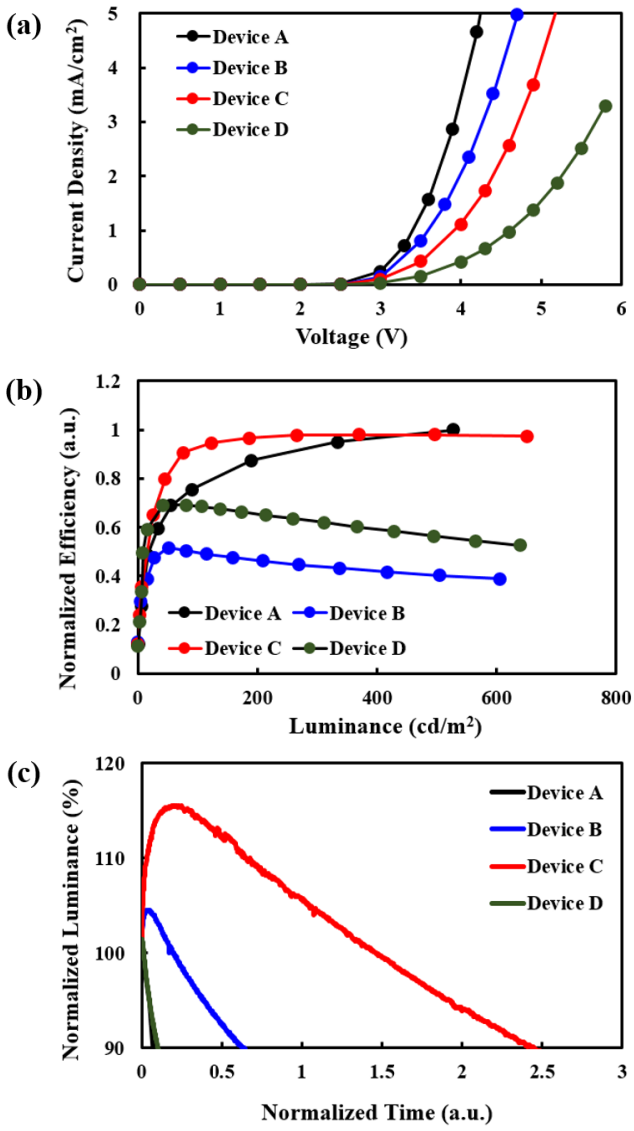

Figure 4. (a) Current density-voltage (J-V) and (b) normalized efficiency-luminance (η-L) characteristics. (c) Operational lifetime of blue EL-QD devices with Device A, B, C, and D.

We also explored strategies to suppress defects at the interface between blue quantum dots (BQDs) and the ZnMgO electron transport layer (ETL) to improve the performance of blue EL-QD devices. These defects, primarily oxygen vacancies, arise due to positive charge (hole leakage) during device operation and act as quenching sites, reducing efficiency and operational lifetime. Introducing halides into ZnMgO proved effective in mitigating these defects by binding to oxygen vacancies and eliminating quenching sites (Figure 5).

Given the challenges of directly doping ZnMgO with halide elements, we instead utilized metal halide compounds—AZP1, AZP2, and AZP3—as dopants, chosen for their availability, solubility, and stability. To check the extent to which each material can generate halide, the cohesive energy of each metal and halide was simulated. Simulation results indicated AZP1's lower cohesive energy made it the most effective halide source (Table 2). Vienna Ab initio Simulation Package (VASP) simulations confirmed halides, rather than metals, effectively passivated ZnMgO defects by eliminating defect-induced energy levels (Figure 6).

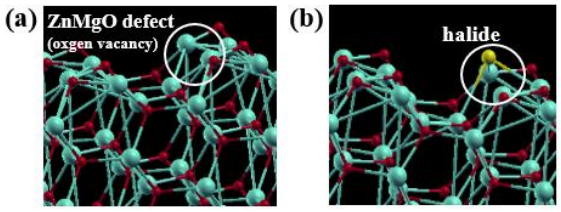

Figure 5. Schematic structures of (a) ZnMgO with defects (oxygen vacancies) and (b) halide-doped ZnMgO.

Table 2. Cohesive energy of metal halide dopants

Metal halide	AZP1	AZP2	AZP3
Cohesive E (eV)	3.69	6.72	5.54

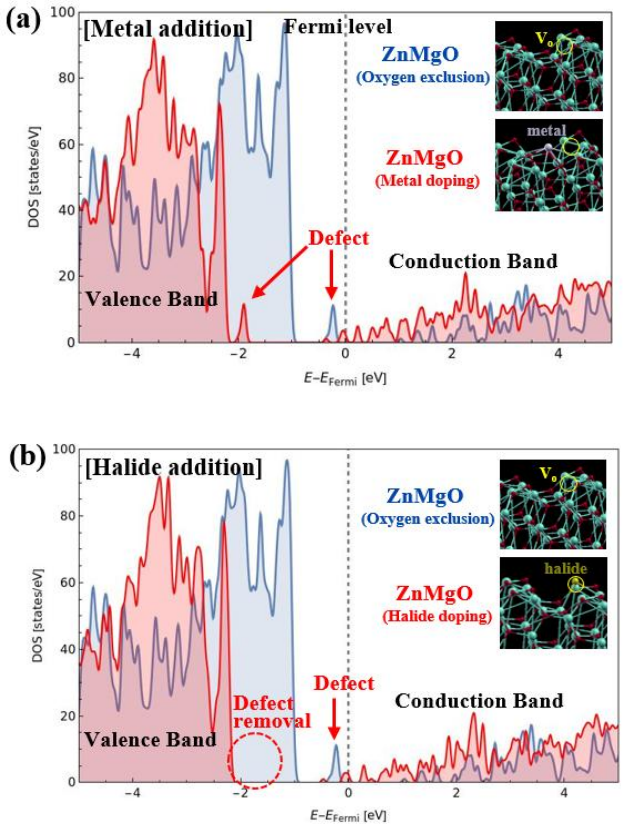

Figure 6. VASP simulation with (a) metal-doped ZnMgO and (b) halide-doped ZnMgO.

Control Device E was prepared by employing the pristine ZnMgO as the ETL, while Devices F, G, and H was prepared by incorporating ZnMgO doped with AZP1, AZP2, and AZP3, respectively. Although the current density-voltage (J-V) characteristics revealed no significant differences in electron

mobility across the devices (Figure 7(a)), notable improvements were observed in efficiency and lifetime. Device F, which utilized AZP1, exhibited the highest efficiency (Figure 7(b), Table 2), attributed to the reduced defects in ZnMgO facilitated by AZP1 doping.

In addition to suppressing ZnMgO defects, halides from the doped ZnMgO may bind to defect sites on the BQD surface, further reducing quenching sites. To confirm this effect, photoluminescence (PL) spectra of BQD/ZnMgO stacked films with and without metal halide doping were compared. As shown in Figure 7(c), the PL intensity of BQDs increased by 1.6 times when metal halide-doped ZnMgO was applied, indicating reduced quenching at the BQD surface. This synergistic reduction of defects in both ZnMgO and BQDs significantly enhanced device efficiency.

Impedance (C-V) measurements were conducted to investigate the influence of halide doping on charge dynamics. The C-V curve at small voltage (2 V) exhibits the geometry capacitance, indicative of leaked carrier accumulation. The C-V curve at higher voltage indicate the carrier dynamics of accumulation and recombination. The increased number of injected hole carriers could enhance the capacitance. On the other hand, recombination of carriers could cause the decrease in capacitance. It was found that hole injection was not affected because there was no change in the position where the capacitance starts to regardless of halide doping. However, when metal halide was applied, the position where capacitance begins to decrease moved toward lower voltage, suggesting improved electron injection, as shown in Figure 7(d). This improvement is attributed to the increased lowest unoccupied molecular orbital (LUMO) energy level of the BQDs after halide treatment, leading to better energy-level alignment with ZnMgO.

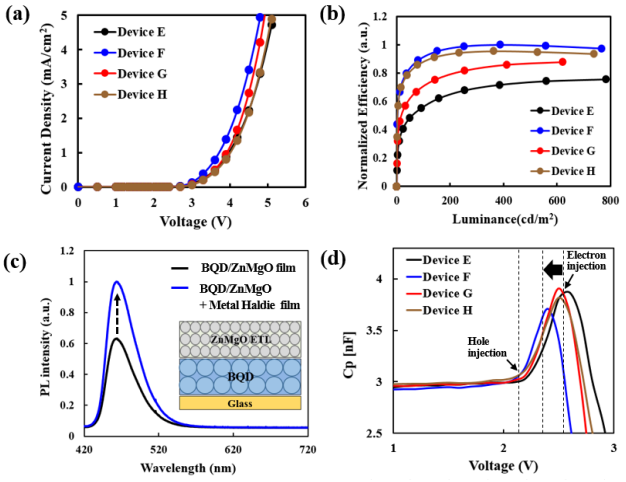

Figure 7. (a) Current density-voltage (J-V) and (b) normalized efficiency-luminance (η-L) characteristics of Devices E ~ H. (c) PL spectra of BQD/ZnMgO stacked films with and without metal halide doping. (d) C-V characteristics of Devices E ~ H.

The operational lifetime of devices was measured (Figure 8). Devices incorporating metal halides demonstrated increased lifetimes compared to the control Device E. Devices G and H, using AZP2 and AZP3, respectively, showed 1.3- and 1.2-fold increases in lifetime. Device F, utilizing AZP1, exhibited a 3.3-fold increase in lifetime, highlighting the superior effectiveness of AZP1. This significant improvement aligns with cohesive energy simulations (Table 2), which identified AZP1 as the most effective halide source due to its lower cohesive energy, enabling greater halide generation and enhanced defect suppression in ZnMgO.

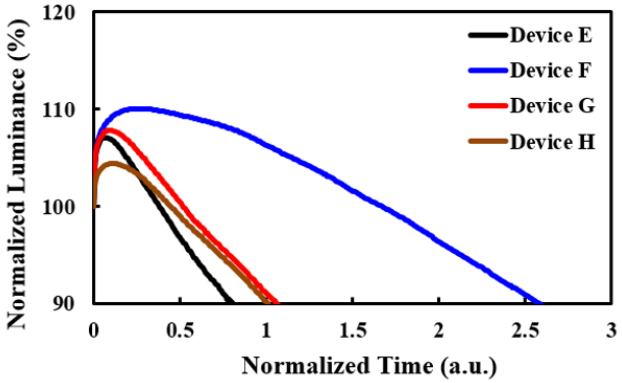

Figure 8. Operational lifetime of blue EL-QD devices of Device E ~ H.

Table 3. Device properties of 18.2-inch all-inkjet-printed EL-QD display panel at a full white luminance of 300 nits.

Color	cd/A	CIEx	CIEy
Red	30.7	0.695	0.305
Green	81.9	0.262	0.716
Blue	6.7	0.132	0.062

We successfully fabricated an 18.2-inch full-color EL-QD display using inkjet printing for all layers, optimizing thicknesses to enhance microcavity effects in the top-emission structure. The RGB devices achieved current efficiencies of 30.7, 81.9, and 6.7 cd/A at a full white luminance of 300 nit, as summarized in Table 3. Figure 9 presents an image of the display panel with a resolution of 202 ppi.

Figure 9. Image of 18.2-inch full-color EL-QD display panel with a 202 ppi resolution.

3. Conclusion

This study demonstrates that ligand engineering, defect control, and optimal device architecture significantly enhance the performance and lifetime of blue EL-QD devices. Ligand engineering on blue ZnSeTe QDs with shorter-chain improves charge injection. The incorporation of AZP1 as a halide dopant effectively suppresses defects in ZnMgO and BQDs, improves charge injection, and enhances energy-level alignment. An 18.2-inch full-color EL-QD display is successfully fabricated using inkjet printing for all layers. These advancements significantly enhanced the performance of blue EL-QD devices, laying the groundwork for commercializing more efficient and durable QD-LED displays.

4. References

[1] Alivisatos, A. P. Semiconductor clusters, nanocrystals, and quantum dots. *Science*. 1996; 271(5251): 933—937.

[2] Kim, J., *et al.*, Recent advances and challenges of colloidal quantum dot light-emitting diodes for display applications. *Adv. Mater*. 2023; 2212220.

[3] Qian, L., *et al.*, 6-2: Invited Paper: Key Challenges towards the Commercialization of Quantum-Dot Light-Emitting Diodes. *SID Int. Symp. Dig. Tech. Papers*. 2017; 48(1): 55—57.

[4] Park M., et al., All inkjet-printed 6.9500 217 ppi active matrix QD-LED display with RGB Cd-free QDs in the top-emission device structure. *J. Soc. Inf. Disp*. 2022;30(5):433–440.

[5] Ha, J., *et al.*, Dual ligand exchange of Cd-free quantum dots and optimal control of ink formulation for improving the performance of all-inkjet-printed quantum dot light-emitting diodes. *J. Soc. Inf. Disp.* 2024; 32(5): 332−340.

[6] Han, C., *et al.*, Inkjet-printed quantum dot light-emitting diodes: Development and challenges for display applications. *J. Soc. Inf. Display*. 2024.

[7] Won, Y.-H. *et al.*, Highly efficient and stable InP/ZnSe/ZnS quantum dot light-emitting diodes, *Nature*. 2019; 575(7784): 634−638.

[8] Yu, P. *et al.*, “Highly efficient green InP-based quantum dot light-emitting diodes regulated by inner alloyed shell component”, *Light Sci. Appl.*, 2022; 11, 162.

[9] Kim, T. *et al.*, “Efficient and stable blue quantum dot light-emitting diode” *Nature*, 2020; 586, 385−389.

[10] Chen, D. *et al.* Electrochemically Stable Ligands of ZnO Electron-Transporting Layers for Quantum-Dot Light-Emitting Diodes. *Nano Lett.* 2023; 23, 1061.

[11] Ghorbani, A. *et al.* Changes in Hole and Electron Injection under Electrical Stress and the Rapid Electroluminescence Loss in Blue Quantum-Dot Light-Emitting Devices. *Small*, 2024; 20, 23045.